A Weakly Solvating Electrolyte to Enable Lithium- and Manganese-Rich Cathode Based Li-Ion Batteries

Qijia Zhu[1,4], Jiayi Xu[1], Cong Liu[1], Wei Jiang[2], Jingtian Yang[1], Zhenzhen Yang[1], Xinqi Chen[6], Seoung-Bum Son[1], Krishna Prasad Koirala[3], Chongmin Wang[3], Owen Wostoupal[1,4], Qian Liu[1], Tao Xu[4]*, and Zhengcheng Zhang[1,5]**

[1]Chemical Sciences and Engineering Division, Argonne National Laboratory, Lemont, IL 60439

[2]Computational Science Division, Argonne National Laboratory, Lemont, IL 60439

[3]Environmental Molecular Sciences Laboratory, Pacific Northwest National Laboratory, Richland, WA 99354

[4]Department of Chemistry and Biochemistry, Northern Illinois University, DeKalb, IL 60115

[5]Pritzker School of Molecular Engineering, The University of Chicago, 5640 S. Ellis Avenue, Chicago, IL 60637

[6]Northwestern University Atomic and Nanoscale Characterization Experimental (NUANCE) Center and Department of Materials Science and Engineering, Northwestern University, Evanston, IL 60208, USA

Corresponding Authors: qian.liu@anl.gov,

Corresponding Authors: txu@niu.edu,

*Corresponding Authors: zzhang@anl.gov

Abstract

Traditional ethylene carbonate (EC)-based electrolytes exhibit strong solvation power at the surface of the layered transition metal oxide cathodes, which accelerate transition metal dissolution. The subsequent migration and deposition of dissolved transition metal species on the

anode surface, leading to significant capacity fading. To overcome this challenge, we report a weakly solvating, all-fluorinated electrolyte designed to mitigate transition metal dissolution. For the first time, the role of electrolyte solvation in suppressing transition metal dissolution is systematically investigated. The tailored electrolyte significantly reduces transition metal dissolution and enhances the electrochemical performance of Li- and Mn-rich (LMR) cathode/graphite cells. This solvation-modulating strategy offers a broadly applicable framework for stabilizing interphases in other earth-abundant cathode chemistries, which similarly demand kinetic protection against interfacial degradation.

Table of Contents (TOC)

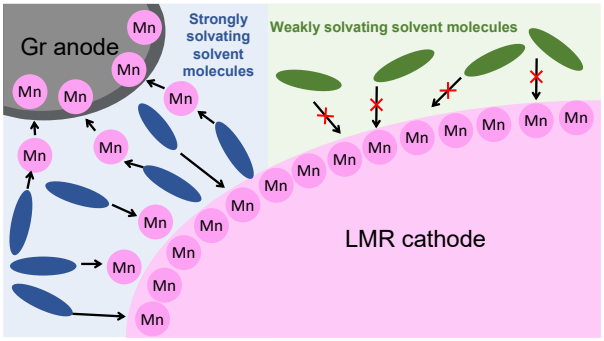

Lithium-ion battery (LIB) has become the most popular electrochemical device, which has undergone rapid technical advances driven by the increasing demand of energy storage. However, high cost remains one of the barriers that impedes the wide adoption of LIB. [1, 2] Lithium- and manganese-rich (LMR) cathode material ($xLi_2MnO_3 \cdot (1-x)\ LiMO_2$ (M = Mn, Ni, etc.)) has emerged as an earth abundant cathode candidate to address cost issue with other notable attributes including high specific capacity (>250 $mAhg^{-1}$ after activation) and environmental compatibility. [3-7] Yet, the practical application of LMR cathode faces several hindrances. To achieve high energy density with increased voltages, LMR cathode triggers irreversible electrolyte decomposition, oxygen release, transition metal ion dissolution and migration, surface corrosion, and other interfacial reactions, deteriorating the electrochemical performance. [6, 8] Manganese-based issues are particularly problematic for this material. Mn^{3+} ions in the cathode are prone to undergo disproportionation reaction producing Mn^{2+}, which can be easily dissolved in the conventional carbonate electrolyte. [9-12] These soluble Mn^{2+} ions have been found to be dissolved into the electrolyte and can further migrate to the graphite anode, deposit on the surface and catalyze electrolyte reduction, resulting in the degradation of the

solid-electrolyte-interphase (SEI) and impedance rise. [13-15] Furthermore, the presence of catalytic Mn could also cause lithium trapping, resulting in further lithium inventory loss and capacity fading. [11, 16-19] Thus, numerous research has been conducted to address transition metal dissolution issues *via* doping and/or surface modification on the material level and interphase modification through electrolyte. [20-24] Surface coating or doping with metal, metal oxides, or polymers was an effective way to mitigate the transition metal dissolution. [14, 25-27] In terms of electrolyte, concentrated electrolytes have been reported by Wu *et. al* and Liu *et. al* to promote the anion dominated formation of a LiF rich cathode-electrolyte interface (CEI).[28, 29] Additives such as tris(trimethylsilyl)phosphite, bis(trimethylsilyl)carbodiimide, and $LiPO_2F_2$ have been also reported to form a stable CEI to mitigate the transition metal dissolution. [30-32]

The interfacial chemistry proposed by Peled in 1979 has been widely used to correlate the battery performance and electrolyte composition/property, where SEI and CEI could well explain the experimental results. [33] However, recent research indicates SEI/CEI theory alone may not be enough to interpret specific experimental results, and coordination structure can also tune the electrode electrochemical behaviors. [34-37] It is widely accepted that traditional carbonate-based electrolytes have strong solvating power with transition metal ions, which undermines the kinetic interfacial stability of LMR cathodes. Altering the solvation energy of electrolyte can impact the driving force of transition metal dissolution into the electrolyte. Therefore, it is crucial to understand the interplay between electrolyte solvation and transition metal dissolution, and its effect to the electrochemical performance of LMR-based battery. Su et al. have demonstrated that with distinct solvation capability, fluorinated carbonates can modulate Li^+ solvation to form a stable interphase for Li metal in a high-voltage NMC811/Li cell.[38] Yet, the correlation between weakly solvating carbonates and the cathode interface, particularly how solvent solvation strength influences transition metal dissolution, has been overlooked. In this work, we investigate the impact of electrolyte solvation capability on transition metals dissolution within a high-energy and high-voltage LMR ($0.3Li_2MnO_3 \cdot 0.7LiMn_{0.5}Ni_{0.5}O_2$)/graphite battery by designing a weakly solvating electrolyte based on fluorinated carbonates. This weakly solvating electrolyte is formulated to offer weakened solvation capability towards transition metal compared to the baseline electrolyte. We also design a preformation experiment in full cells to distinguish between the CEI-induced interphase effect and the electrolyte solvation effect on transition metal dissolution from the LMR cathode. Through this preformation approach, we

isolate and confirm the role of weakened solvation in suppressing transition metal dissolution. As a result, the weakly-solvating electrolyte delivers significantly improved capacity retention, energy retention, and negligible voltage fade in an LMR/graphite full cell. The significance of this weakly solvating electrolyte concept undoubtedly extends to other earth-abundant cathodes and systems beyond lithium-ion, all of which universally require kinetic stability at interface.

In a traditional Li-ion electrolyte, such as Gen2 (1.2 M $LiPF_6$ in ethylene carbonate (EC)/ethyl methyl carbonate (EMC)), solvent molecules solvates the Li^+ with EC dominating the process. [39] Similar to Li^+, transition metal ions like Mn^{2+} and Ni^{2+} get readily solvated in this type of electrolyte as well. As the schematic shown in Figure 1a, due to the solvents' strong solvation capability, a rapid transition metal dissolution manifest in Gen2 electrolyte. The dissolution of Mn^{2+} ions further shifts the disproportionation equilibrium and promotes more Mn^{3+} to produce additional Mn^{2+}, leading to cathode structural damage. The dissolved transition metal ions then migrate to anode surface, resulting in unstable SEI, impedance rise, and Li inventory loss. Hypothetically, this phenomenon could change with a weakly solvating electrolyte that processes weak solvation capability towards transition metal cations. Based on this hypothesis, an all-fluorinated electrolyte denoted as F2 (1.2 M $LiPF_6$ in fluoroethylene carbonate (FEC)/ methyl 2,2,2-trifluoroethyl carbonate (FEMC)) is proposed. In F2, the solvents' coordination capability is weakened by the electron-withdrawing –F and $–CF_3$ groups that reduce the atomic charge on the carbonyl oxygens. A preliminary solubility test (Figure S1) showed that F2 has a lower solubility of both Mn^{2+} and Ni^{2+} than Gen2 as it formed cloudy suspension with undissolved salts when same concentration of $Mn(PF_6)_2$ and $Ni(PF_6)_2$ added in Gen2 formed clear solution. Furthermore, the calculated binding energy of EC and EMC, along with their fluorinated counterparts FEC and FEMC in the presence of Li^+, Mn^{2+} or Ni^{2+}, provides additional support for this hypothesis (Figure 1b-1d). EC shows the strongest binding towards Li^+ at all coordination numbers (n =1- 4), renowned for its ability to solvate Li^+ and thus readily dissociates lithium salt. [40, 41] In contrast, its fluorinated analogue FEC shows a weaker binding compared to EC. Fluorination also causes the lower binding energy of the linear carbonate FEMC. Similar trends in binding capability with transition metal cations Mn^{2+} and Ni^{2+} are observed. Interestingly, the linear carbonates could not form a stabilized structure at coordination number 4. This suggests that steric effect also plays a role in solvation capability.

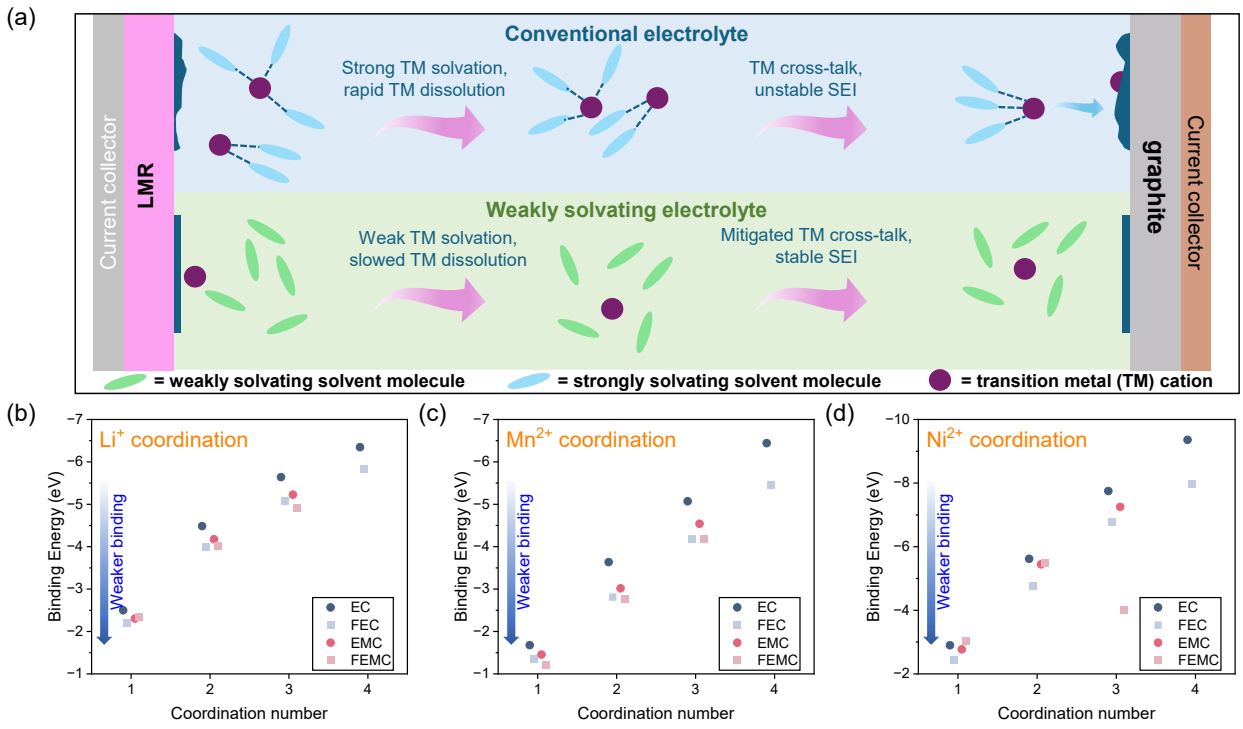

112

113 **Figure 1**. (a) Schematics for the mechanism of weakly solvating electrolyte to prevent transition
114 metal dissolution in an LMR/graphite full cell and (b-d) binding energy calculation of EC, EMC,
115 FEC and FEMC solvent molecules with (b) Li^+, (c) Mn^{2+}, and (d) Ni^{2+} with different
116 coordination numbers.

117

118 The solvation structures of Mn^{2+} and Ni^{2+} ion in Gen2 and F2 were investigated by molecular
119 dynamics (MD) simulation and the results are shown in Figure 2 and Figure S2. 0.2 M $Mn(PF_6)_2$
120 or 0.2 M $Ni(PF_6)_2$ were introduced in both Gen2 and F2 electrolyte to mimic the condition in the
121 battery. At this dilute state (<1.5M) , transition metal solvation is not significantly interfered by
122 Li^+ solvation. For Gen2 electrolyte, in the 1st solvation sheath of Mn^{2+}, EC shows the strongest
123 probability density with Mn^{2+} followed by PF_6^- and EMC (Figure 2a), suggesting EC is dominant
124 in the solvation structure of Mn^{2+}. However, for F2 electrolyte, PF_6^- anion also becomes the
125 dominant species, indicating the weaker solvation capability of fluorinated solvents (Figure 2b).
126 The coordination number of each electrolyte component around Mn^{2+} is summarized in Figure
127 2c. F2 showed a higher PF_6^- coordination number, and a lower linear carbonate (FEMC vs.
128 EMC) coordination number compared to Gen2, while their cyclic carbonates (FEC vs. EC) have

similar coordination numbers. The solvation structure of Ni^{2+} and the coordination number of different electrolyte components show the same trend as evidenced by Figures S2. Overall, based on the MD simulation, the weakened solvent solvation capability of F2 resulted in lower probability of solvent residing in the solvation shell of transition metal cations, which suggests that F2 hinders the dissolution of transition metal cations from LMR cathode into the electrolyte.

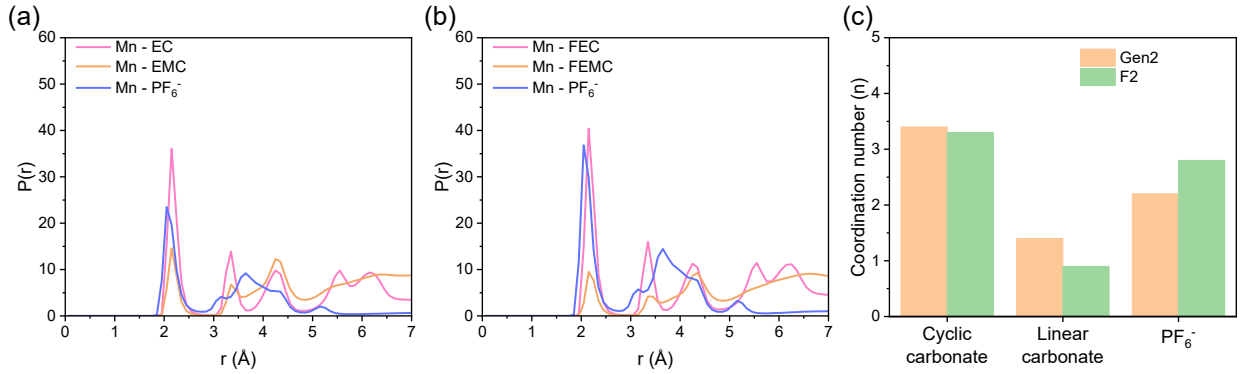

Figure 2. Probability density profiles of electrolyte components surrounding Mn^{2+} in (a) Gen2 electrolyte and (b) F2 electrolyte, and (c) the coordination number of the electrolyte components.

Beyond their distinct solvation characteristics, fluorinated electrolytes have been shown to facilitate the formation of unique fluorine-rich CEI that enhances cathode interface stability [42-44]. In addition, CEI has also been reported to contribute to the inhibition of transition metal dissolution.[14, 28] It then is speculated that in addition to the F2 solvation impact, F2-formed CEI could be another factor affecting transition metal dissolution from LMR cathode. The CEI formed by Gen2 and F2 is examined by X-ray photoelectron spectroscopy (Figure S3) to compare their compositions. The F 1s XPS reveals Li-F (684.5eV) and $Li_xPO_yF_z$ (685.7eV and 686.7 eV) formed by FEC or PF_6^- decomposition and PVDF binder signal at 688.2 eV for LMR cathode formed by both electrolytes. A weak CF_3 signal at 689.7 eV on the F2-formed cathode shows minimal FEMC decomposition, while a more abundant Li-F on the F2-formed cathode indicates a more inorganic rich and protective CEI film. C 1s XPS shows similar signal from both electrode materials, such as C-C (283.6 eV) and C-CF_2 (PVDF, 290.4 eV), and organic species formed by carbonate decomposition in both electrolytes, such as C-C, C-H, C-O, C=O, O-C=O, and O_2-C=O, indicating organic solvent decomposition in both electrolytes. Atomic

concentration further reveals significantly higher percentage of F and significantly lower percentage of C from CEI film formed by F2 (Figure S4), which suggests enhanced protection of cathode interface.[45, 46] The structure and thickness of CEI is further examined by scanning transmission electron microscopy (STEM) analysis (Figure S5). STEM images of LMR particles cycled with Gen2 and F2 indicate that the interphase formed by F2 (~ 2.8 nm) appears to be thinner than the interphase formed by Gen2 (~ 7.1 nm). The structure of CEI interphase demonstrated by STEM images suggests a more crystalline interphase formed by F2, which has been reported to be beneficial for cathode protection.[47, 48]

Since F2 is found to generate a different and more protective CEI on LMR cathode, to evaluate our hypothesis regarding the solvation effect, it is critical to understand the impact of each factor. To achieve this, a preformation experiment was conducted to distinguish the interphase effect and the solvation effect of the electrolyte with LMR/graphite full cell.[49] Figure 3a describes the general procedure of this experiment. LMR and graphite electrodes are precycled by either Gen2 or F2 electrolyte and harvested to acquire formed electrodes. Coin cells are then assembled with the preformed electrodes and fresh electrolytes based on three different electrode-electrolyte combinations presented in Figure 3a: (1). Gen2-formed electrodes and Gen2 electrolyte, denoted as GG, (2). F2-formed electrodes and Gen2 electrolyte, denoted as FG, and (3). F2-formed electrodes and F2 electrolyte, denoted as FF. The combination of Gen2-formed electrodes and F2 electrolyte are ruled out, as the fluorinated F2 may further passivate Gen2-formed electrodes. These coin cells are cycled with an in situ hybrid pulse power characterization (HPPC) testing protocol to check the area specific impedance (ASI) every 25 cycles[50], and the transition metal dissolution was quantified after 100 cycles. The LMR cathodes formed by F2 contain a more robust inorganic-rich interphase, as shown by the XPS and STEM analysis, which helps minimize the further impact of Gen2 on interphase during the following electrochemical tests of FG cell. As shown in Figure 3b, the graphite anode harvested from FG cell showed a 344 ppm of Mn deposition, which corresponds to 73% decreased compared to the 1327 ppm of GG cell, while the graphite harvested from FF cell showed a strikingly low Mn deposition of 32 ppm, which is over 90% less Mn deposition than the FG cell. Besides, the FF cell also shows a significantly reduced amount of Ni in the harvested electrolyte (Figure S6), further demonstrates the effectiveness by combining the F2-interphase and solvation effect. We observed that the majority of Mn dissolved from the LMR cathode has been deposited on the graphite anode, while

substantial amount of Ni has been left in electrolyte (Figure 3c). This observation aligns with previous studies, which reported that Mn is the main culprit of electrolyte decomposition, lithium inventory loss and impedance rise by inducing further electrolyte reduction.[51, 52] While Ni is not reported to be the main contributor of graphite-side lithium inventory loss for the manganese-rich cathode systems, this reduced amount of Ni still correlates to reduced active material loss at the cathode side, reinforcing the improved cathode protection of FF cell. Reduced Mn deposition can be directly related to the electrolyte decomposition and lithium inventory consumption, where FF cell shows the best capacity retention of 93.5%, followed by 88% of FG and 85.5% of GG as shown in Figure 3d. FF cell also delivers the highest average coulombic efficiency (CE) of 99.87% among all cells, supporting its cycle life (expanded long-term CE in Figure S7). Figure 3e-g summarizes the ASI results over cycling from HPPC test. Both GG (Figure 3e) and FG (Figure 3f) exhibited significant ASI rise of more than 140%, resulting in a high final ASI of more than 80 Ω cm^2, while FF (Figure 3g) had negligible ASI increase during cycling.

The transition metal quantification and the ASI results indicate that the combination of an inorganic-rich interphase and a weak solvation is the most effective in mitigating the transition metal dissolution. Although the interphase formed by F2 in the FG cell shows decreased transition metal dissolution than the interphase formed by Gen2 in the GG cell, compared to the weakly solvating F2 electrolyte, the strongly solvating Gen2 could still solvate more transition metal through the cathode interphase, leading to impedance rise and capacity loss. In conclusion, electrolyte solvation capability also plays an important role on top of the protection of an robust interphase in mitigating transition metal dissolution, as only the FF cell, in which F2 was used for both precycling and reassembly, has almost no Mn dissolution.

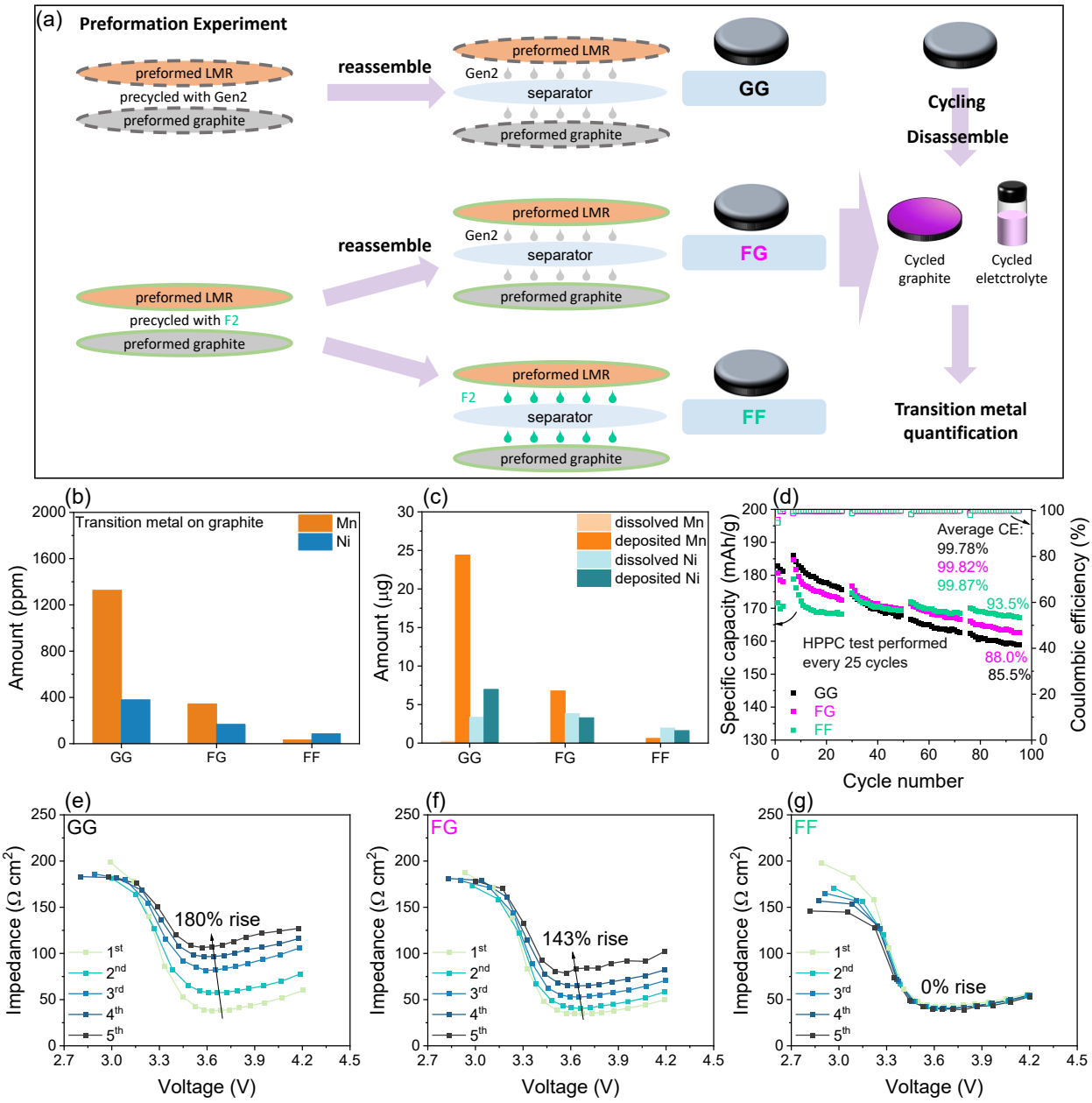

205

206 **Figure 3.** Schematic of the preformation experiment (a), transition metal deposition on graphite
207 anode harvested from reassembled cells in the preformation experiment (b), transition metal
208 dissolved in electrolyte compared with transition metal deposited on graphite anode (c), specific
209 discharge capacity (d) of reassembled cells cycled from 2.5 V – 4.4 V. ASI increase for all
210 reassembled cells calculated from the data of HPPC test protocol. ASI of reassembled cells
211 plotted vs. cell voltage, including GG (e), FG (f), FF (g)

212

LMR/Gr full cell is cycled under HPPC protocol to verify the combined solvation and interphase effect of F2 electrolyte without preformation. As shown in Figure 4a, both Gen2 and F2 electrolytes can deliver over 195 mAh/g capacity at 4.4V after activation. F2 offers a capacity retention of 90% over 100 cycles, outperforming the 75% retention of Gen2. The average CE of F2 (99.93%) has also improved (99.8%) compared to Gen2 (expanded long-term CE in Figure S8). As LMR cathode is well-known for its rapid energy decay due to voltage fade, energy retention and average discharge voltage are plotted in Figure 4b and 4c. F2 retains 89 % specific discharge energy and only shows a 30-mV decay in average discharge voltage after 100 cycles, where Gen2 shows a 200-mV decay and further leads to even lower energy retention of 70%. The ASI evolution of full cells containing Gen2 and F2 without preformation is demonstrated in Figure 4d and 4e. Gen2 suffered from a substantial 393% rise in ASI, while F2 only has 5% ASI rise. To further verify the solvation effect alone, a non-fluorinated weakly solvating electrolyte, EMC (1.2 M $LiPF_6$ in EMC) was also evaluated, which also shows improved cycling performance over Gen2 (Figure S9). Among the three formulations, F2 remains the most effective electrolyte for suppressing ASI growth and transition metal deposition, as fluorination not only promotes an F-rich interphase, but also further reduces the solvation strength of FEC and FEMC (Figure 1b-d).

In the long-term cycling test, F2 again shows a 77% energy retention over 300 cycles, significantly improved from 55% of Gen2 (Figure 4f). Figure 4g and 4h compare the discharge voltage profiles of Gen2 and F2 electrolytes over cycling. Overpotential and voltage fade are clearly observed for Gen2, while no changes are observed for F2 electrolytes. The voltage profiles agree with the average discharge voltage (Figure S10b), suggesting F2 effectively prevents cell impedance rise and voltage fade after 300 cycles. Finally, after 300 cycles of long-term cycling, the 77% capacity retention and 99.91% average CE of F2, compared to the 59% capacity retention and 99.46% average CE of Gen2 (Figure S10a, Figure S10c), validates the superior cycling performance of this electrolyte. Electrochemical impedance spectroscopy (EIS) compares the growth of interfacial resistance (R_{int}) in Gen2 and F2 cell during long-term cycling. A substantial increase of Gen2's R_{int} over 200 cycles is also observed, which can be attributed to continuous electrolyte decomposition buildup at interphase induced by deposited Mn, aligning with the capacity loss and the lower CE during long-term cycling. In contrast, R_{int} of F2 shows a significantly smaller growth over 200 cycles, which can be attributed to inhibited transition metal

dissolution. Gen2 also suffers from a huge rise in charge transfer resistance (R_{ct}) measured at 50% state-of-charge (SOC) compared to F2 (Figure S11), which suggest cathode might suffer from structural degradation when cycled with Gen2, contributing to ASI growth measured by the HPPC test (Figure 4d-e).[53] Compared to recently reported electrolytes in Table S1, F2 enables improved or comparable cycling performance in LMR/graphite full cell while supporting higher loading electrodes with minimal voltage fade. This enhancement in cycling performance, suppression of transition metal and voltage retention, particularly in graphite full-cell configurations, where transition metal dissolution contributes to more SEI degradation and Li inventory loss, represents an important progress in the development of LMR cathode with the design of weakly solvating electrolyte.

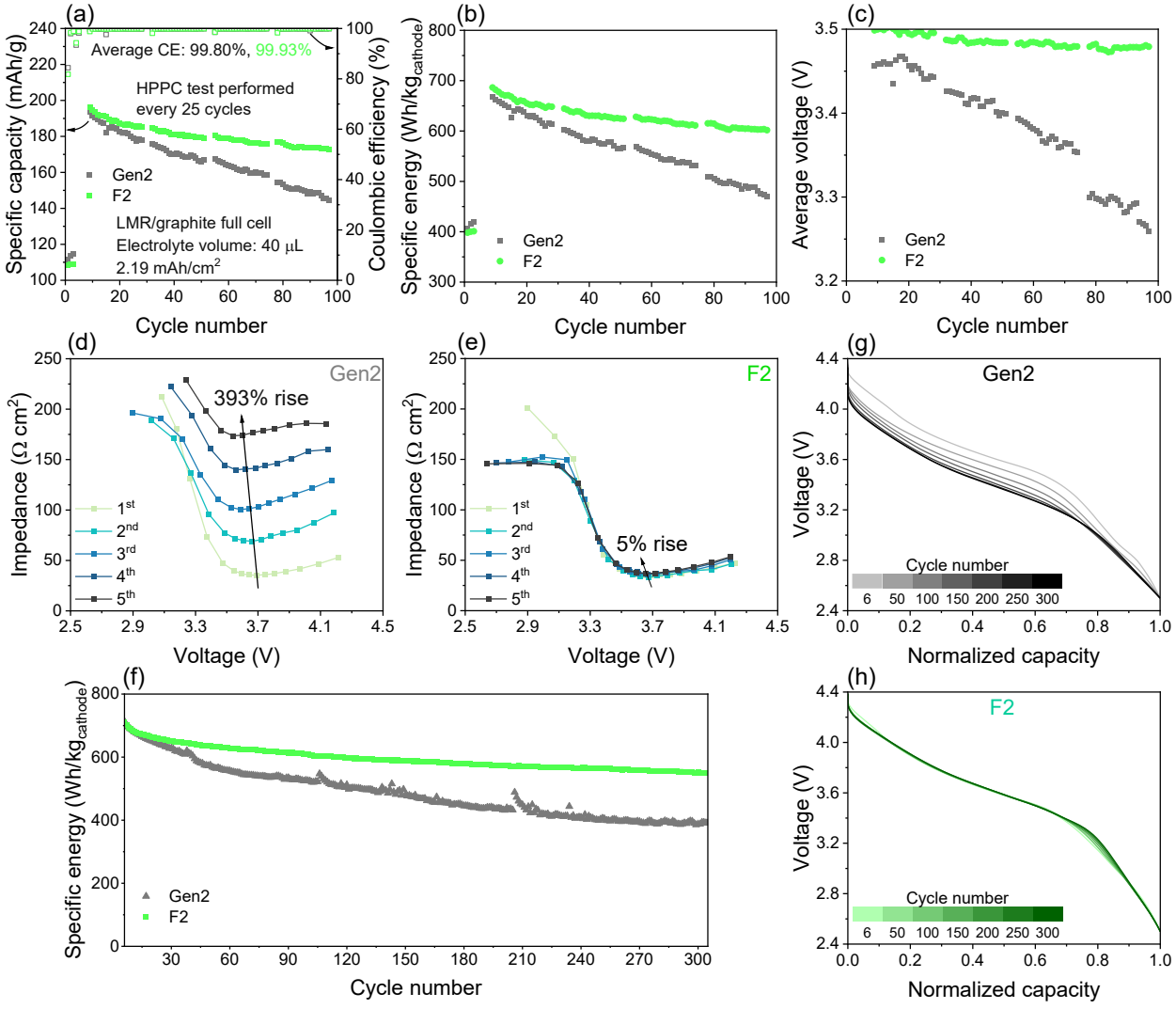

Figure 4. Specific discharge capacity (a), specific discharge energy calculated based on cathode active material (b), discharge average voltage (c) of LMR/graphite full cell cycled with Gen2 and F2 electrolyte for HPPC tests. ASI of Gen2 (d) and F2 (e). Specific discharge energy calculated based on cathode active material (f) of LMR/graphite full cell cycled for 300 cycles from 2.5 V – 4.4 V. Discharge voltage profile evolution based on normalized capacity (normalized using the indicated cycle's total capacity) of LMR/graphite full cell cycled with Gen2 (g) and F2 (h).

The transition metal deposited on anode and dissolved in electrolyte over 300 cycles were quantified and summarized in Figure 5a and Figure S12. 1240 ppm Mn and 532 ppm Ni is measured on the graphite cycled with Gen2, while 477 ppm Mn and 358 ppm Ni is measured on the graphite cycled with F2. This indicates that F2 can effectively reduce both Mn and Ni deposition on the graphite anode by over 60%, and 30%, respectively, compared to Gen2. This reduced transition metal deposited on the anode, especially Mn again correlates to the improved cell performance LMR/Gr full cell. In addition, only 91 ppm Ni is measured in electrolyte harvested from cycled F2 cells, an over 60% decrease compared to the 239 ppm Ni measured in the electrolyte harvested from the cycled Gen2 cell (Figure S12). In contrast to Ni, a very negligible amount of 3 ppm dissolved Mn is detected for Gen2, while no dissolved Mn is detected in F2.

Morphological and compositional analysis of the cycled graphite and anode is conducted to assess the impact of reduced transition metal dissolution on graphite stability (Figure S12-S13). Graphite anode cycled with F2 also shows a cleaner morphology than Gen2 under scanning electron microscopy (SEM) analysis (Figure S13), indicating the less side reactions induced by the deposited transition metal on graphite surface.[54] Time-of-flight secondary ion mass spectrometry (TOF-SIMS) analysis of graphite anode cycled by Gen2 (Figure S14a) further reveals the buildup of a thick SEI layer, attributed to the excessive formation of LiF by electrolyte decomposition. In sharp contrast, the graphite cycled with F2 displays a much thinner SEI layer (Figure S14b), suggesting reduced electrolyte decomposition. XPS results (Figure S15b) are consistent with TOF-SIMS results, showing an excess formation of LiF on Gen2-cycled graphite, which contributes to the increased interfacial resistance observed in Gen2 cell (Figure S11).[55] The drastically decreased amount of transition metal not only on the graphite anode but also in the electrolyte agrees with

the hypothesis that F2 electrolyte prevents dissolution of transition metal from the LMR cathode surface and leading to reduced electrolyte decomposition and SEI component accumulation on the graphite anode.

In addition to the interface and solvation effect, HF is widely reported as a contributing factor to transition metal dissolution.[56] To investigate its role in the F2 electrolyte, an aging test was conducted to assess HF concentration over time. The results, summarized in Table S2, reveal that the HF content in the F2 electrolyte is higher than that in the Gen2 electrolyte after 14 days of aging, likely due to the increased acidity from the proton in FEC. Therefore, while HF can contribute to transition metal dissolution, the interfacial and solvation characteristics of the F2 electrolyte appear to dominate, ultimately leading to reduced transition metal dissolution.

Cathode structure change such as rock-salt phase formation and transition metal migration has been reported to be accompanied by transition metal dissolution.[28, 57] To further assess the mitigation of transition metal dissolution from the LMR cathode by the weakly solvating electrolyte F2, the surface crystal structure of cycled LMR cathode was analyzed by x-ray diffraction (XRD) technique. XRD analysis of cycled LMR shows a more pronounced left-shift of the (003) peak in the LMR cathodes cycled with Gen2 compared to LMR cathode cycled with F2 (Figure S16). The XRD results shows effective LMR cathode protection by F2, as such a left-shift can be attributed to the irreversible lattice distortion and lattice strain due to cycling.[58] High-resolution analysis of surface structural change is observed *via* high-angle annular dark-field scanning transmission electron microscopy (HAADF-STEM) and electron energy loss spectroscopy (EELS). Figure 5b-c presents the STEM image of cycled LMR cathodes. For Gen2 electrolyte, LMR shows rock-salt layer structure near the surface with 10.2-nm thickness that was formed during the cycling. While the LMR cathode cycled with F2 electrolyte only shows a 2.5-nm thick layer of rock-salt like structure, indicating less structure-related degradation incurred during cycling. This structure-related degradation is directly correlated to impedance rise, voltage fade and the transition metal dissolution (Figure 4 and Figure 5a). The electron energy loss spectroscopy (EELS) shown in Figure 5d-e detects the composition change from the surface to the bulk of the particle. The LMR cathode cycled with F2 demonstrated reduced oxygen loss from the surface, whereas the LMR cathode cycled with Gen2 exhibited significant oxygen loss extending from the surface to the bulk of the particles. Moreover, the Mn *L-edge* and

Ni *L-edge* peaks associated with the LMR cathode cycled with F2 is more pronounced near surface, which directly correlates to the mitigated transition metal dissolution by F2. The cathode structure change revealed by STEM and EELS conclude that the mitigated transition metal dissolution with weakly solvating F2 electrolyte slows down the cathode structural damage and phase change, thus further improving cycle life of LMR cathode.

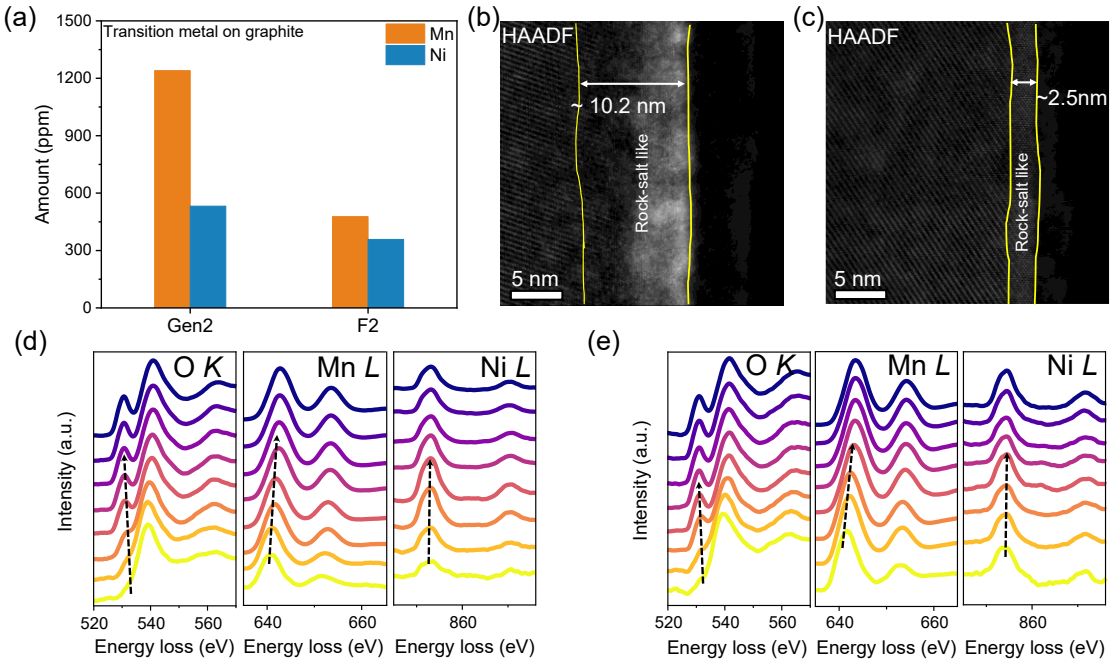

Figure 5. Transition metal deposition (a) on graphite anode harvested from LMR/Gr full cell with fresh electrodes after 300 cycles, HAADF-STEM images of cycled LMR cathode harvested from LMR/Gr full cell using Gen2 (b) and F2 (c). EELS scan from the primary particle surface to the bulk of cycled LMR cathode harvested from LMR/Gr full cell using Gen2 (d) and F2 (e).

Conclusion

In summary, we studied the solvent impact on transition metal dissolution from LMR cathode for the first time and demonstrated with a weakly solvating electrolyte F2, which is composed of FEC and FEMC. In F2, the fluorinated carbonates significantly lower electrolyte solvation capability towards the transition metals (Mn and Ni), therefore lowering the total amount of transition metals dissolving into the electrolyte and reduced on the graphite anode. A

preformation experiment utilizing preformed electrodes and a different cycling electrolyte demonstrated that besides the F-rich preformed interphase, solvation contribution is critical towards the mitigation of transition metal dissolution. F2 elongated cycle life of LMR/graphite full cells when cycled at 4.4V and reduced the amount of transition metal detected on graphite anode by more than 60% after 300 cycles. Reduced transition metal dissolution correlates to the preserved LMR structure, which contributes to enhanced cycle life. This work introduces a new factor for consideration when designing electrolyte for LMR cathode or any high-voltage cathode with severe transition metal dissolution.

Supporting Information

Experimental details, solubility tests, probability density profiles and coordination number of Ni by MD simulation, XPS analysis for formed LMR cathodes, STEM images of LMR cathodes, dissolved transition metal measurement by IC, expanded CE, electrochemical performance and transition metal dissolution analysis for EMC electrolyte, long-term cycling performance of Gen2 and F2, EIS analysis, SEM images of graphite anode surface, TOF-SIMS analysis of cycled graphite anode , XPS analysis for cycled graphite anode, XRD analysis, recent publications, HF concentration measurement.

Author Contributions

Qijia Zhu performed experiments, analyzed data, and drafted the manuscript.

Jingtian Yang performed ion chromatography measurement.

Jiayi Xu and Cong Liu performed DFT calculation.

Wei Jiang performed MD simulation.

Zhenzhen Yang and Seoung-Bum Son performed XPS and SEM experiments, contributed to XPS data analysis.

Xinqi Chen performed TOF-SIMS analysis.

Krishna Prasad Koirala and Chongmin Wang performed STEM experiment.

Owen Wostoupal performed XRD experiment.

Tao Xu* revised manuscript, contributed to discussion.

Qian Liu* and Zhengcheng Zhang* conceived the concept, contributed to discussion, and revised manuscript.

Acknowledgements

This work was funded by the U.S. Department of Energy (DOE), Office of Energy Efficiency and Renewable Energy, Vehicle Technologies Office, particularly from the Earth-abundant Cathode Active Materials (EaCAM) consortium. Support from Tien Duong, Brian Cunningham, Peter Faguy and Mallory Clites of Vehicle Technology Office is gratefully acknowledged. This research used the Leadership Computing Facility resource at Argonne National Laboratory, which is supported by DOE Office of Science under Contract No. DE-AC02-06CH11357. DFT was performed with the computational resources provided by laboratory computing resources center (LCRC). TOF-SIMS analysis made use of the Keck-II facility (RRID: SCR_026360) of Northwestern University's NUANCE Center, which has received support from the SHyNE Resource (NSF ECCS-2025633), the IIN, and Northwestern's MRSEC program (NSF DMR-2308691). The submitted manuscript has been created by UChicago Argonne, LLC, Operator of Argonne National Laboratory.

References

(1) Xiang, J.; Wei, Y.; Zhong, Y.; Yang, Y.; Cheng, H.; Yuan, L.; Xu, H.; Huang, Y. Building Practical High-Voltage Cathode Materials for Lithium-Ion Batteries. *Adv Mater* **2022**, *34* (52), e2200912

(2) Berg, E. J.; Villevieille, C.; Streich, D.; Trabesinger, S.; Novák, P. Rechargeable Batteries: Grasping for the Limits of Chemistry. *Journal of The Electrochemical Society* **2015**, *162* (14), A2468-A2475

(3) Wang, J.; He, X.; Paillard, E.; Laszczynski, N.; Li, J.; Passerini, S. Lithium- and Manganese-Rich Oxide Cathode Materials for High-Energy Lithium Ion Batteries. *Advanced Energy Materials* **2016**, *6* (21),
(4) Schmuch, R.; Wagner, R.; Hörpel, G.; Placke, T.; Winter, M. Performance and Cost of Materials for Lithium-based Rechargeable Automotive Batteries. *Nature Energy* **2018**, *3* (4), 267-278
(5) Zuo, W.; Luo, M.; Liu, X.; Wu, J.; Liu, H.; Li, J.; Winter, M.; Fu, R.; Yang, W.; Yang, Y. Li-rich cathodes for rechargeable Li-based batteries: reaction mechanisms and advanced characterization techniques. *Energy & Environmental Science* **2020**, *13* (12), 4450-4497
(6) Zheng, J.; Myeong, S.; Cho, W.; Yan, P.; Xiao, J.; Wang, C.; Cho, J.; Zhang, J. G. Li- and Mn-Rich Cathode Materials: Challenges to Commercialization. *Advanced Energy Materials* **2016**, *7* (6),
(7) Gan, J.; Wu, Z.; Zheng, C.; Qi, F.; Li, C.; She, L.; Gao, Y.; Li, Z.; Sun, W.; Liu, Y.; et al. Degradation, Intrinsic Microstrains, and Phase Structure Engineering in Lithium-Rich Oxide Cathode Materials. *ACS Energy Letters* **2024**, *9* (12), 6153-6169
(8) Zheng, C.; Feng, J.; Zhang, D.; Zhang, D.; Li, J. Electrochemical In Situ Na Doping to Construct High-Performance Lithium-Rich Cathode. *ACS Energy Letters* **2024**, *9* (4), 1339-1345
(9) Thackeray, M.; Croy, J.; Lee, E.; Gutierrez, A.; He, M.; Park, J. S.; Yonemoto, B.; Long, B.; Blauwkamp, J.; Johnson, C. The quest for manganese-rich electrodes for lithium batteries: strategic design and electrochemical behavior. *Sustainable Energy & Fuels* **2018**, *2* (7), 1375-1397
(10) Gummow, R.; De Kock, A.; Thackeray, M. Improved capacity retention in rechargeable 4 V lithium/lithium-manganese oxide (spinel) cells. *Solid State Ionics* **1994**, *69* (1), 59-67
(11) Joshi, T.; Eom, K.; Yushin, G.; Fuller, T. F. Effects of Dissolved Transition Metals on the Electrochemical Performance and SEI Growth in Lithium-Ion Batteries. *Journal of The Electrochemical Society* **2014**, *161* (12), A1915-A1921
(12) Jiao, S.; Wang, J.; Hu, Y.-S.; Yu, X.; Li, H. High-Capacity Oxide Cathode beyond 300 mAh/g. *ACS Energy Letters* **2023**, *8* (7), 3025-3037
(13) Blyr, A.; Sigala, C.; Amatucci, G.; Guyomard, D.; Chabre, Y.; Tarascon, J. M. Self-Discharge of $LiMn_2O_4$/C Li-Ion Cells in Their Discharged State: Understanding by Means of Three-Electrode Measurements. *Journal of The Electrochemical Society* **1998**, *145*, 194-209
(14) Zhan, C.; Wu, T.; Lu, J.; Amine, K. Dissolution, migration, and deposition of transition metal ions in Li-ion batteries exemplified by Mn-based cathodes – a critical review. *Energy & Environmental Science* **2018**, *11* (2), 243-257
(15) Delacourt, C.; Kwong, A.; Liu, X.; Qiao, R.; Yang, W. L.; Lu, P.; Harris, S. J.; Srinivasan, V. Effect of Manganese Contamination on the Solid-Electrolyte-Interphase Properties in Li-Ion Batteries. *Journal of The Electrochemical Society* **2013**, *160* (8), A1099-A1107
(16) Gilbert, J. A.; Shkrob, I. A.; Abraham, D. P. Transition Metal Dissolution, Ion Migration, Electrocatalytic Reduction and Capacity Loss in Lithium-Ion Full Cells. *Journal of The Electrochemical Society* **2017**, *164* (2), A389-A399
(17) Benedek, R.; Thackeray, M. M. Reaction Energy for $LiMn_2O_4$ Spinel Dissolution in Acid. *Electrochemical and Solid-State Letters* **2006**, *9* (6), A265-A267
(18) Tesfamhret, Y.; Liu, H.; Chai, Z.; Berg, E.; Younesi, R. On the Manganese Dissolution Process from $LiMn_2O_4$ Cathode Materials. *ChemElectroChem* **2021**, *8* (8), 1516-1523

(19) Morin, H. R.; Graczyk, D. G.; Tsai, Y.; Lopykinski, S.; Iddir, H.; Garcia, J. C.; Dietz Rago, N.; Trask, S.; Flores, L.; Son, S.-B.; et al. Transition-Metal Dissolution from NMC-Family Oxides: A Case Study. *ACS Applied Energy Materials* **2020**, *3* (3), 2565-2575
(20) Seaby, T.; Lin, T.-E.; Hu, Y.-X.; Yuan, Q.-H.; Wang, L.-Z. An Analysis of F-doping in Li-rich Cathodes. *Rare Metals* **2022**, *41* (6), 1771-1796
(21) Sun, Z.; Xu, L.; Dong, C.; Zhang, H.; Zhang, M.; Liu, Y.; Zhou, Y.; Han, Y.; Chen, Y. Enhanced Cycling Stability of Boron-doped Lithium-rich Layered Oxide Cathode Materials by Suppressing Transition Metal Migration. *Journal of Materials Chemistry A* **2019**, *7* (7), 3375-3383
(22) Hestenes, J. C.; Marbella, L. E. Beyond Composition: Surface Reactivity and Structural Arrangement of the Cathode–Electrolyte Interphase. *ACS Energy Letters* **2023**, *8* (11), 4572-4596
(23) Qin, M.; Zeng, Z.; Ma, F.; Gu, C.; Chen, X.; Cheng, S.; Xie, J. Doping in Solvation Structure: Enabling Fluorinated Carbonate Electrolyte for High-Voltage and High-Safety Lithium-Ion Batteries. *ACS Energy Letters* **2024**, *9* (6), 2536-2544
(24) Zhao, J.; Zhang, X.; Liang, Y.; Han, Z.; Liu, S.; Chu, W.; Yu, H. Interphase Engineering by Electrolyte Additives for Lithium-Rich Layered Oxides: Advances and Perspectives. *ACS Energy Letters* **2021**, *6* (7), 2552-2564
(25) Cao, Z.; Li, Y.; Shi, M.; Zhu, G.; Zhang, R.; Li, X.; Yue, H.; Yang, S. Improvement of the Cycling Performance and Thermal Stability of Lithium-Ion Batteries by Coating Cathode Materials with Al_2O_3Nano Layer. *Journal of The Electrochemical Society* **2017**, *164* (2), A475-A481
(26) Lee, Y.-S.; Shin, W.-K.; Kannan, A. G.; Koo, S. M.; Kim, D.-W. Improvement of the Cycling Performance and Thermal Stability of Lithium-Ion Cells by Double-Layer Coating of Cathode Materials with Al_2O_3 Nanoparticles and Conductive Polymer. *ACS Applied Material Interfaces* **2015**, *7* (25), 13944-13951
(27) Yang, S.; Yan, P.; Bao, W.; Zhu, H.; Cai, X.; Zhao, L.; Zhang, Y.; Lin, W.; Deng, Y.; Wu, Y.; et al. Surface Magnesium Substitution at Spinel Lithium Manganate 8a Tetrahedral Sites for Suppressed Manganese Dissolution and Enhanced Cycle Stability. *ACS Energy Letters* **2023**, *8* (10), 4278-4286
(28) Liu, W.; Li, J.; Li, W.; Xu, H.; Zhang, C.; Qiu, X. Inhibition of Transition Metals Dissolution in Cobalt-free Cathode with Ultrathin Robust Interphase in Concentrated Electrolyte. *Nature Communications* **2020**, *11* (1), 3629
(29) Wu, S.; Li, C.; Zhang, J.; Wang, P.; Zhao, D.; Quan, Y.; Sun, J.; Cui, X.; Li, S. Inhibition of transition-metal dissolution with an inert soluble product interface constructed by high-concentration electrolyte. *iScience* **2023**, *26* (7), 107052
(30) Mai, S.; Xu, M.; Liao, X.; Hu, J.; Lin, H.; Xing, L.; Liao, Y.; Li, X.; Li, W. Tris(trimethylsilyl)phosphite as Electrolyte Additive for High Voltage Layered Lithium Nickel Cobalt Manganese Oxide Cathode of Lithium Ion Battery. *Electrochimica Acta* **2014**, *147*, 565-571
(31) Lan, J.; Zheng, Q.; Zhou, H.; Li, J.; Xing, L.; Xu, K.; Fan, W.; Yu, L. e.; Li, W. Stabilizing a High-Voltage Lithium-Rich Layered Oxide Cathode with a Novel Electrolyte Additive. *ACS Appl Mater Interfaces* **2019**, *11* (32), 28841-28850
(32) Jiang, B.; Li, J.; Luo, B.; Yan, Q.; Li, H.; Liu, L.; Chu, L.; Li, Y.; Zhang, Q.; Li, M. $LiPO_2F_2$ Electrolyte Additive for High-performance Li-rich Cathode Material. *Journal of Energy Chemistry* **2021**, *60*, 564-571

(33) Peled, E. The Electrochemical Behavior of Alkali and Alkaline Earth Metals in Nonaqueous Battery Systems - The Solid Electrolyte Interphase Model *Journal of the Electrochemical Society* **1979**, *126*, 2047
(34) Ming, J.; Cao, Z.; Wahyudi, W.; Li, M.; Kumar, P.; Wu, Y.; Hwang, J.-Y.; Hedhili, M. N.; Cavallo, L.; Sun, Y.-K.; et al. New Insights on Graphite Anode Stability in Rechargeable Batteries: Li Ion Coordination Structures Prevail over Solid Electrolyte Interphases. *ACS Energy Letters* **2018**, *3* (2), 335-340
(35) Zhou, L.; Cao, Z.; Wahyudi, W.; Zhang, J.; Hwang, J.-Y.; Cheng, Y.; Wang, L.; Cavallo, L.; Anthopoulos, T.; Sun, Y.-K.; et al. Electrolyte Engineering Enables High Stability and Capacity Alloying Anodes for Sodium and Potassium Ion Batteries. *ACS Energy Letters* **2020**, *5* (3), 766-776
(36) Zhou, L.; Cao, Z.; Zhang, J.; Cheng, H.; Liu, G.; Park, G. T.; Cavallo, L.; Wang, L.; Alshareef, H. N.; Sun, Y. K.; et al. Electrolyte-Mediated Stabilization of High-Capacity Micro-Sized Antimony Anodes for Potassium-Ion Batteries. *Adv Mater* **2021**, *33* (8), e2005993
(37) Li, Q.; Cao, Z.; Wahyudi, W.; Liu, G.; Park, G.-T.; Cavallo, L.; Anthopoulos, T. D.; Wang, L.; Sun, Y.-K.; Alshareef, H. N.; et al. Unraveling the New Role of an Ethylene Carbonate Solvation Shell in Rechargeable Metal Ion Batteries. *ACS Energy Letters* **2020**, *6* (1), 69-78
(38) Su, C.-C.; He, M.; Cai, M.; Shi, J.; Amine, R.; Rago, N. D.; Guo, J.; Rojas, T.; Ngo, A. T.; Amine, K. Solvation-protection-enabled high-voltage electrolyte for lithium metal batteries. *Nano Energy* **2022**, *92*,
(39) Hou, T.; Fong, K. D.; Wang, J.; Persson, K. A. The Solvation Structure, Transport Properties and Reduction Behavior of Carbonate-based Electrolytes of Lithium-ion Batteries. *Chemical Science* **2021**, *12* (44), 14740-14751
(40) Lee, H.; Hwang, S.; Kim, M.; Kwak, K.; Lee, J.; Han, Y.-K.; Lee, H. Why Does Dimethyl Carbonate Dissociate Li Salt Better Than Other Linear Carbonates? Critical Role of Polar Conformers. *The Journal of Physical Chemistry Letters* **2020**, *11* (24), 10382-10387
(41) Hall, D. S.; Self, J.; Dahn, J. R. Dielectric Constants for Quantum Chemistry and Li-Ion Batteries: Solvent Blends of Ethylene Carbonate and Ethyl Methyl Carbonate. *The Journal of Physical Chemistry C* **2015**, *119* (39), 22322-22330
(42) Zhang, X.; Zhao, J.; Lee, G. H.; Liang, Y.; Wang, B.; Liu, S.; Wang, E.; Yang, W.; Yu, H. Bulk oxygen stabilization via electrode-electrolyte interphase tailored surface activities of Li-rich cathodes. *Advanced Energy Materials* **2023**, *13* (2), 2202929
(43) Li, T.; Zhang, X.-Q.; Shi, P.; Zhang, Q. Fluorinated solid-electrolyte interphase in high-voltage lithium metal batteries. *Joule* **2019**, *3* (11), 2647-2661
(44) Liu, X.; Li, Y.; Liu, J.; Wang, H.; Zhuang, X.; Ma, J. 570 Wh kg⁻ 1-Grade Lithium Metal Pouch Cell with 4.9 V Highly Li+ Conductive Armor-Like Cathode Electrolyte Interphase via Partially Fluorinated Electrolyte Engineering. *Advanced Materials* **2024**, *36* (24), 2401505
(45) Ouyang, D.; Wang, K.; Pang, Y.; Wang, Z. A fluorinated carbonate-based electrolyte for high-voltage Li(Ni0.8Mn0.1Co0.1)O2 lithium-ion cells. *Journal of Power Sources* **2022**, *529*,
(46) Fan, X.; Ji, X.; Chen, L.; Chen, J.; Deng, T.; Han, F.; Yue, J.; Piao, N.; Wang, R.; Zhou, X.; et al. All-temperature batteries enabled by fluorinated electrolytes with non-polar solvents. *Nature Energy* **2019**, *4*, 882-890
(47) Bai, P.; Ji, X.; Zhang, J.; Zhang, W.; Hou, S.; Su, H.; Li, M.; Deng, T.; Cao, L.; Liu, S. Formation of LiF-rich cathode-electrolyte interphase by electrolyte reduction. *Angewandte Chemie International Edition* **2022**, *61* (26), e202202731

(48) Zhang, Q.; Ma, J.; Mei, L.; Liu, J.; Li, Z.; Li, J.; Zeng, Z. In situ TEM visualization of LiF nanosheet formation on the cathode-electrolyte interphase (CEI) in liquid-electrolyte lithium-ion batteries. *Matter* **2022**, *5* (4), 1235-1250
(49) Tornheim, A.; Sahore, R.; He, M.; Croy, J. R.; Zhang, Z. Preformed Anodes for High-Voltage Lithium-Ion Battery Performance: Fluorinated Electrolytes, Crosstalk, and the Origins of Impedance Rise. *Journal of The Electrochemical Society* **2018**, *165* (14), A3360-A3368
(50) Long, B. R.; Rinaldo, S. G.; Gallagher, K. G.; Dees, D. W.; Trask, S. E.; Polzin, B. J.; Jansen, A. N.; Abraham, D. P.; Bloom, I.; Bareño, J.; et al. Enabling High-Energy, High-Voltage Lithium-Ion Cells: Standardization of Coin-Cell Assembly, Electrochemical Testing, and Evaluation of Full Cells. *Journal of The Electrochemical Society* **2016**, *163* (14), A2999-A3009
(51) Shin, H.; Lee, Y. K.; Lu, W. Structural degradation of graphite anode induced by dissolved manganese ions in lithium-ion batteries. *Journal of Power Sources* **2022**, *528*, 231223
(52) Solchenbach, S.; Hong, G.; Freiberg, A. T. S.; Jung, R.; Gasteiger, H. A. Electrolyte and SEI Decomposition Reactions of Transition Metal Ions Investigated by On-Line Electrochemical Mass Spectrometry. *Journal of The Electrochemical Society* **2018**, *165* (14), A3304-A3312
(53) Jung, S. K.; Gwon, H.; Hong, J.; Park, K. Y.; Seo, D. H.; Kim, H.; Hyun, J.; Yang, W.; Kang, K. Understanding the Degradation Mechanisms of LiNi0.5Co0.2Mn0.3O2 Cathode Material in Lithium Ion Batteries. *Advanced Energy Materials* **2013**, *4* (1),
(54) Joshi, T.; Eom, K.; Yushin, G.; Fuller, T. F. Effects of dissolved transition metals on the electrochemical performance and SEI growth in lithium-ion batteries. *Journal of the electrochemical society* **2014**, *161* (12), A1915
(55) Huey, Z.; Ha, Y.; Frisco, S.; Norman, A.; Teeter, G.; Jiang, C.-S.; DeCaluwe, S. C. Multi-modal characterization methods of solid-electrolyte interphase in silicon-graphite composite electrodes. *Journal of Power Sources* **2023**, *564*, 232804
(56) Sahore, R.; O'Hanlon, D. C.; Tornheim, A.; Lee, C.-W.; Garcia, J. C.; Iddir, H.; Balasubramanian, M.; Bloom, I. Revisiting the Mechanism Behind Transition-Metal Dissolution from Delithiated LiNixMnyCozO2 (NMC) Cathodes. *Journal of The Electrochemical Society* **2020**, *167* (2), 020513
(57) Cao, B.; Li, T.; Zhao, W.; Yin, L.; Cao, H.; Chen, D.; Li, L.; Pan, F.; Zhang, M. Correlating Rate-Dependent Transition Metal Dissolution between Structure Degradation in Li-Rich Layered Oxides. *Small* **2023**, *19* (42), 2301834
(58) Zhu, W.; Hovington, P.; Bessette, S.; Clément, D.; Gagnon, C.; Gariépy, V.; Provencher, M.; Mathieu, M.-C.; Trudeau, M. L.; Vijh, A. Design parameters for enhanced performance of Li1+ xNi0. 6Co0. 2Mn0. 2O2 at high voltage: a phase transformation study by In Situ XRD. *Journal of The Electrochemical Society* **2021**, *168* (10), 100526